Drift Chamber CDR Status

F. Grancagnolo

INFN – Lecce

30.08.2017

Drift Chamber CEPC Note

CEPC NOTE

August 29, 2017

Draft version 0.1

1

A Drift Chamber Proposal for CEPC

Content

Contents

1 Introduction **3**

2 Physics Requirements and Performance Goal **3**

3 Overview **3**

4 Mechanical Design **3**
- 4.1 Layer Structure 3
- 4.2 Drift Cell Structure 4
- 4.3 Wire Choice 4
- 4.4 Electrostatic Stability 4
- 4.5 Gas Mixture 4

5 Cluster Counting/Timing Techniques **4**
- 5.1 Cluster Timing for improved spatial resolution 4
- 5.2 Cluster Counting for particle identification 5
- 5.3 Requirements for Cluster Timing/Counting 5

6 Front-end electronics **6**
- 6.1 Signal amplifier and digitizer 6
- 6.2 Data reduction and cluster analysis 6

7 Drift chamber material budget **6**
- 7.1 Mechanical Structure 6
- 7.2 Gas mixture and wires contribution 6

Content

9 Expected performance **6**
- 9.1 Aging . . . 6
- 9.2 Measured spatial resolution . . . 6
- 9.3 Transverse momentum resolution . . . 6
- 9.4 Angular resolutions . . . 6
- 9.5 Momentum resolution . . . 6
- 9.6 Particle identification . . . 6

10 Simulation and Reconstruction **6**
- 10.1 Simulation framework . . . 7
- 10.2 Geometry description . . . 7
- 10.3 Hit digitization . . . 7
- 10.4 Vertex detector and pre-shower integration . . . 7
- 10.5 Track finding and fitting . . . 7

11 Predicted Performance **7**
- 11.1 Beam related backgrounds . . . 7
- 11.2 Cell occupancy from background and physics events . . . 7
- 11.3 Discussion about geometry optimization based on occupancy . . . 7
- 11.4 Efficiency with montecarlo truth and with track finding . . . 7
- 11.5 Longitudinal and transverse impact parameter resolution . . . 7
- 11.6 Momentum resolution . . . 7
- 11.7 Angular resolutions . . . 7
- 11.8 Particle identification . . . 7
- 11.9 ZH events: Z and H invariant mass in dimuon . . . 7

12 Conclusion **7**

Text in *Word*

Introduction

The drift chamber (DCH) is designed to provide good tracking, high precision momentum measurement and excellent particle identification by cluster counting. Main peculiarity of the drift chamber is its high transparency, in terms of radiation lengths, obtained thanks to the novel approach adopted for the wiring and assembly procedures. Original ancestor of the DCH design is the drift chamber of the KLOE experiment [1], more recently culminated in the realization of the MEG2 drift chamber [2].

Physics requirements and performance goals

To be filled.

Overview

The DCH is a unique volume, high granularity, all stereo, low mass cylindrical drift chamber, co-axial to the 2T solenoid magnetic field. It extends from an inner radius R_{in} = 0.35 m to an outer radius R_{out} = 2 m, for a length L = 4 m.
It is made of 112 co-axial layers, at alternating sign stereo angles and arranged in 24 identical azimuthal sectors. The square cell size varies between 12.0 and 14.5 mm. The total number of drift cells is 56,448.
The angular coverage, for tracks originated at the origin and efficiently reconstructed in space, is 97%.

Mechanical design

Here goes a description of the end plate structure: elm shaped end plate; spokes; wire PCB and spacers; tension recovering scheme; inner cylinder; outer carbon fiber sandwich; sealing scheme.

Text in *Word*

Drift chamber layout

Layer structure

The active volume of the drift chamber is divided in 14 co-axial super-layers, each one composed of 8 layers, at alternating sign stereo angles, for a total of 112 layers, arranged in 24 identical azimuthal sectors.
The innermost 8 layers, constituting the first super-layer, contain $N_1 = 192$ drift cells (8 per sector) each. In order to maintain an approximately constant cell size, the number of drift cells in each consecutive super-layer is incremented by 48 (by 2 in each sector): $N_i = 192 + (i-1) \times 48$, up to $N_{14} = 816$ (34 drift cells per sector), for a total of 56,448 drift cells.
The width of the cell, approximately square, varies from about 12 mm at the innermost layer to about 14.5 mm at the outermost layer.
The stereo angle is generated by stringing the wires between two points on the end plates at the same radius and mutually displaced by two sectors ($2\times\alpha_i = \pm 30°$, see Fig. Stereo).
Thus, the stereo angles increase linearly with the layer radius from 50 to 250 mrad. Because of this configuration, the cell size at the end plates results larger by about 3.5%, with respect to the cell size at z = 0, maintaining, though, its aspect ratio identical to 1 at any z.
Each layer consists of three wire sub-layers: an inner and an outer cathode sub-layers made of 40 μm diameter Ag coated Al field wires and a middle anode sub-layer made of alternating sense (20 μm diameter Au coated W) and field shaping (50 μm diameter Ag coated Al) wires. Two consecutive layers are oriented at opposite stereo angles. The outer cathode sub-layer of each layer lies at the same radius as the inner cathode sub-layer of its radially adjacent layer, thus forming a dense equipotential mesh of cathode wires (Fig. Layers). Its envelope in space forms a rotational hyperboloid surface. The resulting large ratio of field to sense wires of 5:1, besides assuring uniformity of response longitudinally, allows for thinner field wires, thus reducing the total mass of the chamber and the tension load on the end plates.

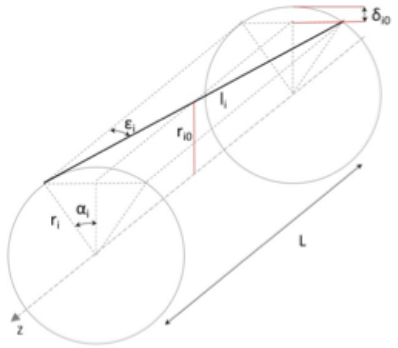

Fig. Stereo

Drift cell structure

A reasonable single electron signal (pulse height of the order of 6 mV), with the configuration described in Fig. Layers (sense to field wires capacitance C = 8 pF/m), is obtained at a gas amplification of 6×10^5, corresponding to 100 fCoul charge on the sense wire, or 10 nCoul/m linear charge density, assuming a charge spread of the order of 10 μm.
These values are compatible with 1.25 KV sense wire positive potential with respect to the field wires. The necessary electric field of about 200 KV/cm on the sense wire surface is reached with a 20 μm diameter sense wire.
In order to avoid generating uncorrelated noise due to positive ions amplification, the electric field on the surface of the field wires must be kept below 20 KV/cm. It is, therefore, necessary that the surface of all field wires surrounding a sense wire be, at least, ten times larger than the sense wires surface. In the described configuration of Fig. Layers, with 5 field wires per sense wire, the resulting diameter of the field wires must, then, be at least twice the sense wire diameter: 40 μm.

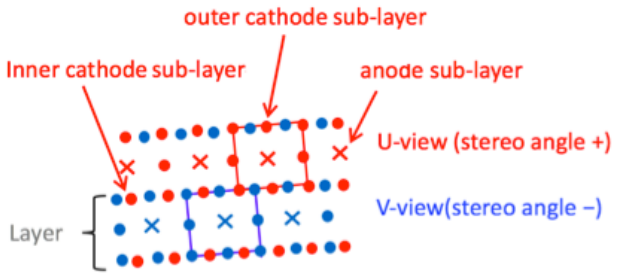

Fig. Layers

Wire choice

Gas amplification considerations recommend 20 μm sense wire and 40 μm field wire diameters.
Wire description: materials, coatings, producer, stress-strain, plots.

Text in *Word*

Electrostatic stability

Electrostatic stability condition for a sense wire, radius r, length L, at Voltage V_0 with respect to the surrounding field wires placed at distance w and with mutual capacitance per unit length:

$$C = \frac{2\pi\varepsilon}{\ln\left(\frac{w}{r}\right)}$$

is reached when the wire mechanical tension T is above the value:

$$T > \frac{C^2 V_0^2 L^2}{4\pi\varepsilon w^2}$$

In this case,
Here goes the discussion about chamber length and wire choice and gravitational sagitta. Also choice of different wire material for longer chamber.

Gas mixture

A helium-based gas mixture is chosen to minimize multiple scattering and energy losses. Also, helium is fairly insensitive to X-ray background and exhibits a small Lorentz angle in magnetic field. The relevant properties of the gas mixture, either measured directly, or computed with transport equations, are listed in Table Gas. The drift velocity as a function of the electric field is shown in Fig Vdrift.

Table Gas. Properties of the 90%He – 10% iC4H10 gas mixture

Number of primary clusters (per m.i.p.)	12.3 cm^{-1}
Number of total clusters (per m.i.p.)	19 cm^{-1}
Drift velocity (E = 0.4-1.0 KV/cm)	1.5-2.4 cm/μs
Lorentz angle (E = 0.4-1.0 KV/cm, B = 2T)	15°-20°
Longitudinal diffusion	170 μm/√cm
Radiation length	1300 m

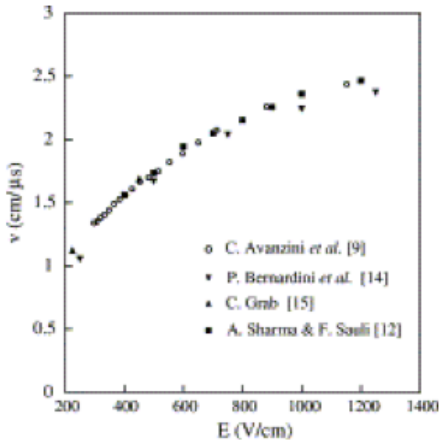

Fig. Vdrift

The meager density of primary clusters produced in a helium based gas mixture affects in a biased way the spatial resolution, particularly for small impact parameters, however, it allows exploiting the possibility of correcting the bias, with statistical considerations, by measuring the arrival time of each individual ionization cluster, as illustrated in the next paragraph.

Text in *Word*

Cluster Counting/Timing Techniques

Cluster Timing for improved spatial resolution

Fig. Signal left shows the signal generated on a 20 μm sense wire by a m.i.p. crossing a 8 mm diameter drift tube (an illustration of the ionization process is presented in Fig. Tube), filled with 90%He – 10%iC_4H_{10} gas mixture, at a gain of 5×10^5 and read out by a 1 GHz, 2 GSa/s, 8 bit digitizer, after a ×10 gain preamplifier. Single electron pulses, as well as multiple electron cluster pulses, are clearly identifiable by a peak finder algorithm (in Fig. Signal right, the result of PEAKFIT software, applied to the signal at left, is shown) and their amplitudes and times can reliably be reconstructed.
From the ordered sequence of the electrons arrival times and from their amplitude, considering the average time separation between ionization clusters and the time spread due to diffusion, one can thus reconstruct the most probable sequence of the cluster drift times:

$$\left\{t_i^{cl}\right\} \quad i=1,N_{cl}$$

The cluster timing technique, given such a sequence, exploits the drift time distribution of all clusters to determine, with statistics based algorithms, the most probable impact parameter, thus reducing the bias and the average drift distance resolution with respect to those obtained by the first cluster method alone.

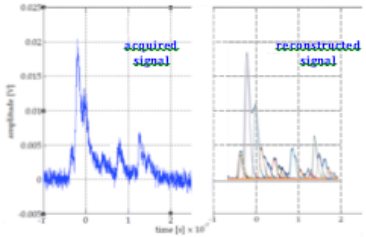

Fig. Signal

Fig. Tube

In Fig. Bias, one can see the result of the application of several algorithms to the sequence of cluster times. The Maximum Possible Spacing (MPS) algorithm is the one that corrects the bias in the most effective way and reduces it by about 100 μm in the most critical region around the sense wire.

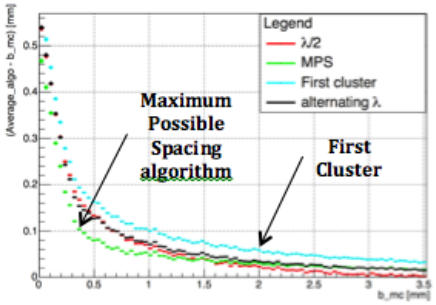

Fig. Bias

Text in *Word*

Cluster Counting for particle identification

Thanks to the Poisson nature of the ionization process, by counting the total number of ionization clusters N_{cl} along the trajectory of a charged track in a drift chamber, one can reach, in principle, a relative resolution on $dN_{cl}/dx = N_{cl}^{-1/2}$. The data shown in Fig. PId, were taken in a 200 MeV/c momentum beam of muons and pions selected by time of flight. A 2.6 cm square drift tube, oriented at 45° with respect to the beam direction (to avoid corrections due to space charge effects), filled with a 95%He – 5%iC_4H_{10} gas mixture (N_{cl} = 9/cm), instrumented with a 25 μm sense wire (gas gain 2×10^5), readout through a high bandwidth (1.7 GHz, ×10 gain) preamplifier and digitized with a 2 GSa/s 1.1 GHz, 8 bits digital scope, was used to collect the data. By merging together 100 different signals, belonging to a muon or to a pion, one is able to reproduce the effects of a 3.7 m long track (*NIM A386 (1997) 458-469* and references therein).

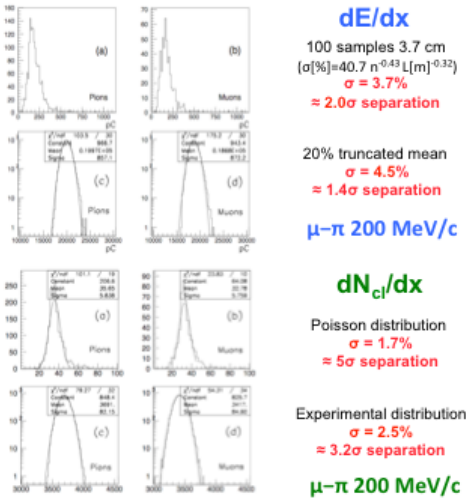

dE/dx

100 samples 3.7 cm
$[\sigma[\%]=40.7\ n^{-0.43}\ L[m]^{-0.32}]$
σ = 3.7%
≈ 2.0σ separation

20% truncated mean
σ = 4.5%
≈ 1.4σ separation

μ–π 200 MeV/c

dN_{cl}/dx

Poisson distribution
σ = 1.7%
≈ 5σ separation

Experimental distribution
σ = 2.5%
≈ 3.2σ separation

μ–π 200 MeV/c

Fig. PId

Fig. PId a) and b) top show the typical Landau distribution of the integrated collected charge over a single signal, respectively for pions and muons. The best resolution in dE/dx one can, in theory, achieve under these conditions (gas at NTP), according to Walenta's parameterization, with n = 100 and L = 3.7 m is σ(dE/dx)/(dE/dx) = 3.7%, corresponding to a 2.0σ mu/pi separation. By truncating 20% of the largest dE/dx samples, in order to obtain normal distributed values, experimentally, one gets instead σ(dE/dx)/(dE/dx) = 4.5%, corresponding to a 1.4σ mu/pi separation.

The number of clusters in the 3.7 cm samples is shown in Fig PId a) and b) bottom. The misidentification of the Poisson distributed number of clusters is indicated by the asymmetric tails, both in the single 3.7 cm sample (a) and b)) and in the distributions (c) and d)) summed over 100 samples. This bears, as a consequence, the worsening of the resolution from a theoretical value, σ = 1.7%, corresponding to a 5.0σ mu/pi separation, to the experimental value σ = 2.5%, corresponding to a 3.2σ mu/pi separation.

This simple exercise demonstrates the potentialities of the cluster counting method for particle identification, able to achieve a relative resolution better by a factor two with respect to the traditional method of the dE/dx truncated mean.

Requirements for Cluster Timing/Counting

The use of helium based gas mixtures, thanks to the sparse number of primary ions per unit length and to the slower drift velocity, makes the application of the cluster counting/timing techniques particularly favorable. In these mixtures, average drift time difference between consecutive clusters goes from a few ns, for clusters close to the sense wire, where drift velocity is at its highest values, to tens of ns for clusters at several mm from the sense wire. As shown in Fig. Signal, a ×10 gain preamplifier and a 1 GHz, 2 GSa/s, 8 bit digitizer are, therefore, sufficient to guarantee an efficient cluster identification and, consequently, a sizeable improvement on spatial resolution (below 100 μm) and a very effective particle identification ($\sigma(dN_{cl}/dx)/(dN_{cl}/dx) \approx 2.5\%$).

Text in *Word*

Front-end electronics

Signal amplifier and digitizer

Main requirement for the front-end preamplifier is to

Data reduction and cluster analysis

From FIRB.

Drift chamber material budget

Mechanical Structure

Inner and outer cylinders, end plates: wire cage and gas envelope.

Gas mixture and wires contribution

Gas 90/10 helium/isobutane and MEG2 wires

Expected performance

Aging

Results from MEG2.

Measured spatial resolution

Published results from MEG2.

Transverse momentum resolution

Analytical calculations.

Angular resolutions

Analytical calculations.

Momentum resolution

Analytical calculations.

Particle identification

Analytical calculations.

Simulation and Reconstruction

Simulation framework

Gianfranco: description of frameworks used.

Geometry description

Gianfranco: description of geometry used.

Hit digitization

Gianfranco: da MEG2.

Vertex detector and pre-shower integration

Gianfranco: description of vertex detector and pre-shower.

Track finding and fitting

Geanfit and preliminary algorithms.

Predicted Performance

Beam related backgrounds.
Cell occupancy from background and physics events
Discussion about geometry optimization based on occupancy
Efficiency with montecarlo truth and with track finding
Longitudinal and transverse impact parameter resolution
Momentum resolution
Angular resolutions
Particle identification
ZH events: Z and H invariant mass resolution in dimuon

Drift Chamber Prototype TEST @ PSI
Sept. 13-27, 2017